scientific reports

OPEN

Analysis of tumour oxygenation in model animals on a phosphorescence lifetime based macro-imager

Alexander V. Zhdanov[1,3], Rajannya Sen[1,3], Ciaran Devoy[2,3], Liang Li[1], Mark Tangney[2] & Dmitri B. Papkovsky[1✉]

Monitoring of tissue O_2 is essential for cancer development and treatment, as hypoxic tumour regions develop resistance to radio- and chemotherapy. We describe a minimally invasive technique for the monitoring of tissue oxygenation in developing grafted tumours, which uses the new phosphorescence lifetime based Tpx3Cam imager. CT26 cells stained with a near-infrared emitting nanoparticulate O_2 probe NanO2-IR were injected into mice to produce grafted tumours with characteristic phosphorescence. The tumours were allowed to develop for 3, 7, 10 and 17 days, with O_2 imaging experiments performed on live and euthanised animals at different time points. Despite a marked trend towards decreased O_2 in dead animals, their tumour areas produced phosphorescence lifetime values between 44 and 47 μs, which corresponded to hypoxic tissue with 5–20 μM O_2. After the O_2 imaging in animals, confocal Phosphorescence Lifetime Imaging Microscopy was conducted to examine the distribution of NanO2-IR probe in the tumours, which were excised, fixed and sliced for the purpose. The probe remained visible as bright and discrete 'islands' embedded in the tumour tissue until day 17 of tumour growth. Overall, this O_2 macro-imaging method using NanO2-IR holds promise for long-term studies with grafted tumours in live animal models, providing quantitative 2D mapping of tissue O_2.

Back in 1909, a markedly reduced response to the radiation of the skin with limited blood supply highlighted the significance of tissue oxygenation for radiotherapy[1]. The studies conducted by Gray in 1950s have shown that hypoxia causes resistance to radiation in various tissue models, including human lung cancers[2,3]. Mechanistically, upon irradiation of deoxygenated tissue, low levels of Reactive Oxygen Species (ROS) are produced, such that ROS-induced damage of DNA, proteins and lipids under hypoxia becomes much lower than at physiological normoxia. Thus, being an intrinsic feature of many tumours[4–7], hypoxia has emerged as an attractive target for cancer therapy[8].

Although tumours are very different by their origin and metabolism, the underlying mechanism of deep deoxygenation is common: rapid tumour growth with uncontrolled cell proliferation, increases consumption of oxygen (O_2) and reduces its supply via blood flow to the 'core' regions of the tumour. The growing demand for O_2 is partially compensated by increased angiogenesis in tumour tissues (e.g. due to activation of HIF-dependent signalling[9]), however O_2 levels the tumours still remain low and heterogenous. The reported median O_2 levels in human tumours vary from 0.3 to 0.4% in pancreatic and prostate cancers to 1.9–2.2% in lung cancer[4]. Core tumour areas with critically low pO_2 start to fail their normal physiological functions and become necrotic[10]. Necrotisation, in turn, leads to subsequent inflammatory response and poor prognosis[11,12].

Over the years various techniques have been applied to study tumour hypoxia[6,13–15], however reliable quantitative data on O_2 levels in various human and mammalian tumours (reviewed in McKeown[4]) were mostly produced on microelectrode based Eppendorf pO2 histography system. For many years, this invasive technique has been considered as 'gold standard' for tissue O_2 measurement, although it requires special expertise to achieve correct insertion of the electrode in tumour regions[16–18]. Still, the electrode disrupts the tissues and provides only point measurements rather than whole distribution of O_2 in the tumour. The alternative non-invasive approaches include Positron emission tomography (PET), Near-infrared spectroscopy (NIRS), Photoacoustic spectroscopy,

[1]School of Biochemistry and Cell Biology, University College Cork, Pharmacy Building, College Road, Cork, Ireland. [2]Cancer Research @UCC, University College Cork, Cork, Ireland. [3]These authors contributed equally: Alexander V. Zhdanov, Rajannya Sen and Ciaran Devoy. ✉email: d.papkovsky@ucc.ie

Magnetic resonance imaging (MRI), Electron paramagnetic resonance spectroscopy (EPR) and Phosphorescence Lifetime Imaging (PLIM).

PET is an in vivo tomographic imaging technique where organic molecular markers labelled with positron-emitting radioisotopes are used to measure the extent of hypoxia in tumours. The tracers are usually injected intravenously or inhaled. As soon as the tracer reaches the target, PET scanner with an array of photoelectric crystals is used to quantify the hypoxia. However, PET has low anatomical resolution (~ 4–5 mm)[19–22].

NIRS is an optical technique that continuously monitors regional tissue oxygenation by measuring haemoglobin saturation with the transmission and absorption of light. The technique uses light in near infrared region to perform real time measurements. The drawback of these systems is that they measure bound O_2 in vasculature, rather than free O_2 and tissue pO_2[23–26].

Photoacoustic imaging is a non-invasive hybrid imaging modality which allows optical contrast sensing with acoustic resolution in deep tissue[27,28]. In this method, photon energy from a short laser pulse is absorbed by the sample and converted into heat, leading to a thermal-elastic expansion. This induces a rise of local pressure and emission of acoustic waves. Photoacoustic imaging detects these acoustic signals generated by optical absorption from endogenous chromophores (deoxy-Hb, or exogenous contrast agents such as, nanoparticles and organic dyes. Although the method generates high resolution images, it is limited by optical attenuation[29] and inaccuracies at depth beyond 1 mm[30].

MRI can image tumour pO_2 in vivo, usually upon intravenous injection of perfluorocarbon or fluorinated nitroimidazole probes. This method, referred as fluorine-19 (^{19}F) oximetry, can report on absolute values of O_2 concentration[31–33]. Blood oxygen level-dependent MRI (BOLD-MRI) measures fluctuations in the amount of oxygen bound to haemoglobin in the blood[34–36], though it does not provide absolute O_2 concentrations. Dynamic contrast-enhanced MRI (DCE-MRI) is another promising method that can measure blood flow and blood volume in tissues[37–39].

EPR spectroscopy also uses exogenous probes to obtain information about tissue oxygenation[40–42]. Radical probes with unpaired electrons are sensitive to tissue environment, including O_2. Changes in the EPR signal due to the interaction of the probe with O_2 are used to determine pO_2. However, the paramagnetic markers used show significant toxicity which limits their use in humans. Development of low toxicity probes and dedicated instrumentation for clinical applications will increase the utility of this technique.

Phosphorescence Lifetime Imaging Microscopy (PLIM) of O_2 is a minimally invasive technique. It involves injection of a suitable phosphorescent probe into the vasculature or in tissue areas, which can then provide quantitative measurement of tissue pO_2[43–45]. Several PLIM setups and phosphorescent probes have been described for mapping O_2 in animal models. Thus, dendrimeric structures were chemically attached to the emitter, to encapsulate and protect it from interaction with sample components, and control the rate of oxygen quenching. Oxyphors R2 and G2 belong to this group[46,47], so as PtP-C343, the two-photon excitable phosphorescent nanoprobe[48], and the latest enhanced two-photon excitable Oxyphor 2P probe which provides high sensitivity and O_2 imaging at depths up to 600 μm[49]. However, these probes are rather complex and usually administered intravenously in live animals or by pressure injection into tissues. These probes cannot effectively penetrate cells and biological membranes and do not allow long-term use (only several hours).

NanO2-IR is another type of O_2 sensing probe which consists of polymeric nanoparticles impregnated with a near-infrared phosphorescent dyes. NanO2-IR is cell-permeable, it can stain different cells and tissues and be applied topically[50,51]. Potentially, it can provide quantitative visualisation of O_2 in long-term imaging experiments with animal models.

Recently we have described an imager based on the Tpx3Cam chip and TCSPC hardware, which was optimised for macroscopic PLIM imaging and biological applications[52]. The imager can detect individual photons and record their arrival time and time over threshold at each pixel simultaneously with good spatial and temporal resolution. This imager, in conjunction with the NanO2-IR probe, was successfully applied to imaging of O_2 concentration in tissue samples ex-vivo[53–56]. In this study, we aim to demonstrate the Tpx3Cam imager in in vivo experiments—to map O2 distribution and tissue hypoxia in grafted tumours of laboratory animals (mice).

Materials and methods

The cell-permeable nanoparticle probe NanO2-IR was synthesised as described previously[57,50]. Dulbecco's modified Eagle medium (DMEM), foetal bovine serum (FBS), paraformaldehyde (PFA), low melting point agarose, and all other chemicals were from Millipore-Sigma (Burlington, MA, USA).

Cell culture and staining with NanO2-IR

Murine colorectal carcinoma CT26 cells (the American Collections of Cell Cultures) were maintained in high glucose DMEM supplemented with 10% FBS, 2 mM L-glutamine, 100 U/ml penicillin/100 μg/ml streptomycin, and 10 mM HEPES, pH 7.2 (complete DMEM), in humidified atmosphere of 95% air and 5% CO_2 at 37 °C.

For staining, cells were seeded in wells of a 6-well plate (Sarstedt, Ireland) at 8×10^5 cells per well and allowed to grow for 24 h in complete DMEM, then washed with serum-free DMEM, and incubated for 18–20 h with different concentrations of NanO2-IR in serum-free DMEM. Cells were then washed sequentially with serum-free DMEM, complete DMEM and PBS, trypsinised, transferred into serum-free DMEM and prepared for injection in animals.

As a viability reporter, total ATP levels in CT26 cells were analysed with CellTiter-Glo assay kit (Promega), according to the manufacturers' protocol. Briefly, cells were incubated with different concentrations of NanO2-IR in FBS-free DMEM (100 μl, 18 h in a CO_2 incubator), then the cells were lysed with 100 μl of CellTiterGlo reagent. After intensive shaking (2 min, 37 °C), the samples (200 μl) were incubated for 4 min, transferred into

wells of white 96-well plates (Greiner Bio One) and analysed on a Victor 2 plate reader under standard luminescence settings.

Experiments with animals (mice)

All animal procedures were performed according to the European Union Directive 2010/63/EU amended by Regulation (EU)2019/1010, as well as national ethical guidelines of the Health Products Regulatory Authority (HPRA), under project authorisation AE19130/I285. Health status of all mice was monitored daily for the duration of experiments. There were no deaths outside the humane euthanasia. Mice were humanely euthanized by cervical dislocation after tumours reached the size of 1.5×1.5 cm in diameter.

Probe delivery and tumour induction in mice

Mice were kept at constant room temperature (22 °C) with natural day/night light cycle in a conventional animal unit. Standard laboratory food and water were provided ad libitum. Before experiments, the mice were given an adaptation period of at least 7 days. Female Balb/C (CT26 models) mice in good condition, disease free, weighted 16–22 g at 6–8 weeks of age (Envigo, U.K.), were included in the experiments. For routine tumour induction, a minimum tumorigenic dose of cells (1×10^5 of non-stained CT26 cells or a mixture of 1×10^5 non-stained cells and 1×10^5 stained with NanO2-IR cells (unless otherwise stated) suspended in 200 µl serum-free culture medium were injected subcutaneously (SC) into the right flank. Following tumour establishment, tumours were allowed to grow and develop, and they were monitored daily. Tumour volume was measured and calculated according to the formula: $V = (L \times W^2)/2$, where L is the longest diameter of the tumour (length) and W is the longest diameter perpendicular to diameter L (width).

Imaging tissue O_2 on the Tpx3Cam imager

The PLIM macro-imager (described in Sen et al.[52]) comprised a Tpx3Cam optical camera (Amsterdam Scientific Instruments, The Netherlands), coupled by means of a Cricket adapter (Photonis, France) with an image intensifier (Photonis, France), a 760 ± 50 nm bandpass emission filter (25 mm, Edmund Optics, York, UK) and a 50 mm lens Navitar NMV-50M11 (Thorlabs). A bright 5 mm red LED (627 nm, Parts Express, Springboro, OH) was used for pulsed excitation of grafted tumours in animals. The Cricket adaptor provided a compact and flexible design to the imager which allowed 360° rotation. In this study the imager was used in an upright orientation, and it provided spatial resolution of 39.4 µm in X–Y plane and averaged signals in Z-dimension with maximal depth of light penetration into tissue of ~ 0.5 mm[52].

On the day of imaging at defined time-points, mice were taken from the animal facility for biological and imaging experiments. One animal was taken, immobilised by concussion and tissue O_2 was immediately imaged in vivo. The mouse was then euthanized by cervical dislocation and immediately subjected to O_2 analysis in live post-mortem tissue, taking a series of five PLIM imaging sessions with 6 min intervals. During the imaging, the animal was kept in a petri dish on a temperature-controlled stage with a block heater (Thermo Fisher Scientific, Waltham, MA) set at 37 °C, such that tumour area was facing the camera. This procedure was repeated for each animal in the group. Body temperature of the mouse at different time points of the imaging procedure was traced using rectal T-probe Ellab DM852 (Medical Precision) and IR DT8803 (Duratool) thermometer.

PLIM images were acquired at LED power 2.4 V, pulse width 500 ns and integration time 20 s. Other operational parameters and imaging focus were adjusted with Sophy software provided by Amsterdam Scientific Instruments. The raw data was acquired by a custom designed software and then post-processed with a C-language program code. *Tri2* software was used to fit the data with two-exponential decay functions and determine the lifetime values.

Imaging on a confocal PLIM microscope

For the analysis of NanO2-IR distribution in tissue, tumours were excised immediately after the post-mortem animal imaging and fixed in 4% paraformaldehyde in PBS (30 min at room temperature). The samples were then washed in PBS, embedded into low melting point agarose (4% in PBS) and sectioned on a Leica VT1000s vibratome (Leica Biosystems, Wetzlar, Germany) to produce ~ 500 µm thick slices of the middle part of tumour cross-section, which were imaged. Prior to confocal imaging, NanO2-IR isles inside the slices were visualised with a camera of iPhone 14 (Apple, CA).

Microscopy of the NanO2-IR probe was performed on the confocal FLIM/PLIM imaging system (Becker&Hickl, Germany): at 37 °C for live cells using a $20 \times/1.0$ W-Plan Apochromat dipping objective, and at 22 °C for tissue slices using a $5 \times/0.25$ FLUAR objective. Phosphorescence lifetime signals were measured in air-saturated conditions (for the cells and tumour tissues) and after chemical deoxygenation by the addition of 5 mg/ml Na_2SO_3 and 5 mg/ml K_2HPO_4 (tumour tissues). The imaging system comprised an upright microscope Axio Examiner Z1 with heated incubator and stage (T = 37 °C), motorized Z-axis control (all from Carl Zeiss, Germany)[58], connected to a DCS-120 confocal scanner (B&H), a 405 nm BDL-405-SMNi picosecond diode laser (B&H), and an R10467U-40 photon counting detector, with > 30% quantum efficiency at 400 ± 700 nm (Hamamatsu Photonics, Japan). Excitation and emission light was separated with a 405 nm dichroic mirror and a 716 ± 20 nm emission filter (both from Semrock, Rochester, NY, USA). The laser and scanner were connected to the TCSPC detection hardware (B&H), with scanning resolution 256×256 pixel. Image acquisition was controlled by MicroToolBox software, version 2011 (Carl Zeiss) and SPCM software, version 9.81 (B&H). The PLIM data was then processed in SPCImage software, version 8.4 (B&H) to determine lifetime values. Numerical values corresponding to PLIM colour images and lifetime distribution histograms were exported in Microsoft Excel. Figures were assembled using ImageJ, Adobe Photoshop and Illustrator software.

Ethical approval

All animal procedures were performed under authorisations issued by the Health Products Regulatory Authority (HPRA, Ireland), under project authorisation AE19130/I285, in accordance with the European Communities Council Directive (2010/63/EU) and amended by Regulation (EU)2019/1010. All experimental protocols were approved by the Animal Experimentation Ethics Committee of the University College Cork. The reporting in the manuscript follows the recommendations in the ARRIVE guidelines.

Results and discussion

Optimisation of NanO2-IR probe delivery and tumour growth

First, we optimised conditions for delivery of NanO2-IR probe in mice and its incorporation in tumours formed by CT26 cells injected subcutaneously. For that, we examined cell staining and toxicity effects of the probe on cultured cells, and optimised conditions for producing grafted tumours stained with NanO2-IR. This work allowed us to choose staining concentrations of NanO2-IR for cell staining that produce measurable phosphorescence during tumour growth, which was monitored for up to 17 days.

The CellTiterGlo cytotoxicity assays did not show major effects on cells of the NanO2-IR probe used at concentrations 0–200 µg/ml and incubation time 18 h (Fig. 1A). However, microscopy analysis revealed some long-term effects of NanO2-IR: the cells treated with > 50 µg/ml probe for 20 h did not proliferate and died within 20–30 h after the staining (Fig. S1A). Even at 50 µg/ml, the probe strongly reduced cell proliferation rate, which gradually increased at lower NanO2-IR concentrations.

These in vitro results suggested that development of tumours from cells pre-stained with NanO2-IR at > 50 µg/ml, or even lower concentrations, could be problematic. Therefore, we tested proliferation of 1:1 mixtures of non-stained and stained cells with different concentrations of NanO2-IR. This strategy markedly improved cell proliferation in vivo: even in the presence of cells stained with 200 µg/ml NanO2-IR, the non-stained cells grew well and formed tumours (Fig. S1B). So, injection of a mixture of stained and non-stained cells produced efficient tumour growth and sufficient quantities of the probe in tumour tissue. As an alternative, we also administered non-stained cells mixed with NanO2-IR just before the injection.

Next, we examined cell staining efficiency at different NanO2-IR concentrations. When analysing phosphorescence of NanO2-IR in the stained CT26 cells on a confocal PLIM microscope, we noticed that intensity signals do not increase proportionally with probe concentration used for the staining. Thus, when NanO2-IR levels in the medium increased from 25 µg/ml to 200 µg/ml, signals produced by cells increased by less than 50% (Fig. 1B,C).
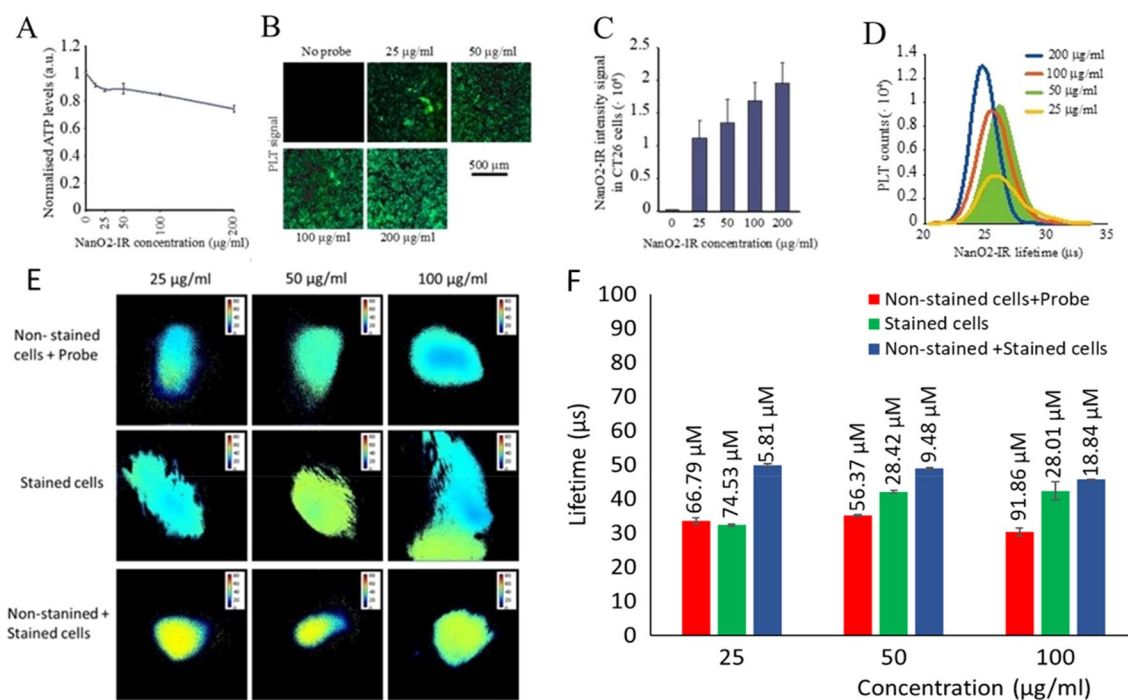
Figure 1. Optimisation of NanO2-IR delivery to grafted tumours in mice. (**A**) Effects of the different concentrations of NanO2-IR probe (indicated, incubation time 18 h, N = 6) on the viability of cultured CT26 cells. Viability was analysed with a CellTiter-Glo kit, which measures total cellular ATP levels. (**B**, **C**) Confocal microscopy analysis of staining efficiency of CT26 cell at different concentrations of NanO2-IR (18 h, N = 6). (**D**) Distribution histogram of lifetime values, calculated for the cells stained with different concentrations of NanO2-IR (as in **B**, **C**). (**E**) Post-mortem PLIM images of NanO2-IR in tumour tissue, taken with Tpx3Cam imager; the probe was delivered as specified. (**F**) Bar charts comparing probe lifetime values and calculated O_2 concentrations for the different trials (as in **E**, N = 3).

When used at concentrations 25–200 µg/ml, NanO2-IR produced high and sustained intensity signals in cells and stable lifetime values, which were usable for the analysis of tissue oxygenation in mice on the PLIM macro-imager (Fig. 1D). To prove this, we injected the cells with the probe in the right flank areas of freshly sacrificed animals, and then conducted imaging of these areas. NanO2-IR probe was delivered into animal tissue at three different concentrations (25, 50, 100 µg/ml) using three different methods: (1) non-stained cells mixed with the probe; (2) cells stained with probe; and (3) 1:1 mixture of the non-stained and stained cells. For the first two methods, the injections were made to post-mortem animals and images were taken within 20 min. For the third method, (called here Preliminary Trial), the injections were made in live animals, and the images were taken on the days 4, 7 and 10 of tumour growth—from 3 mice on each Day. For each animal, the first measurement was taken from live anaesthetized animal (time zero), and then five repeated measurements over 6–30 min were taken from euthanized animal. Thus, the total number of PLIM images in this Trial, N = 54 ($3 \times 6 \times 3$).

Figure 1E shows PLIM images for the three methods of delivery at three different concentrations of NanO2-IR probe, taken immediately after the animals were euthanised, on Day 4 of tumour growth. Figure 1F demonstrates the corresponding lifetime values and O_2 concentrations, calculated using the calibration curve and transformation equation generated for the NanO2-IR probe in solution at 30 °C (Figure S4, Supplementary Information). From these experiments, it appears that the mixture of non-stained and cells stained with all three probe concentrations produced the most stable lifetime signals and lowest O_2 values, which were expected in the tissue of euthanised animals.

Based on the results of cell staining, analysis of proliferation and post-mortem animal imaging in the Preliminary Trial, for in vivo O_2 imaging experiments of the Main Trial we have chosen the injection of 1:1 mixture of stained with 50 µg/ml probe and non-stained cells (Fig. 2A).

In vivo and post-mortem analysis of O_2 levels in tumours

We ruled out repeated imaging of live animals under anaesthesia, which is known to alter functioning of the respiratory system and oxygenation state of animal tissue[59]. Such a procedure would also require sterilizing the imager and placing it inside the animal house, which was not feasible. In our experimental procedure, the imager was set up next to the animal facility. For imaging, test animals were placed on a heated stage. As tested with
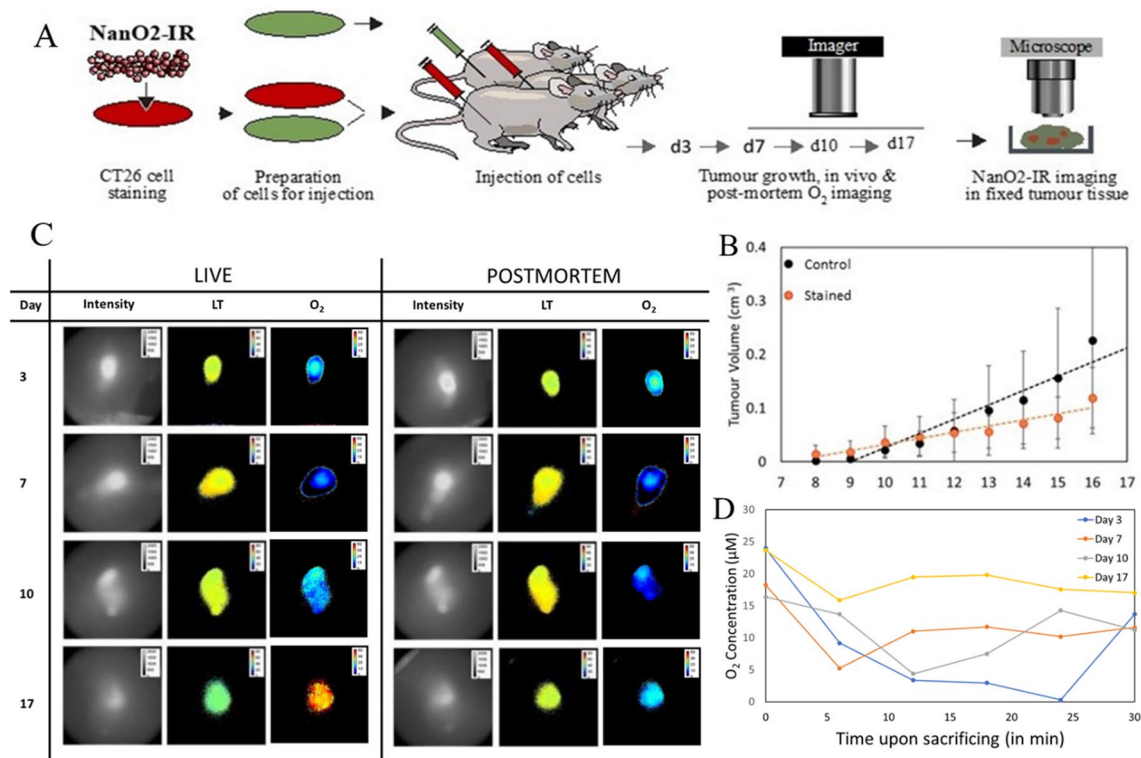
Figure 2. Imaging analysis of tumour oxygenation. (**A**) The scheme of in vivo and post-mortem O_2 imaging of tumour tissue of mice. CT26 cells stained with NanO2-IR (50 µg/ml, 18 h) were mixed with non-stained CT26 cells (1:1) and injected immediately in mice subcutaneously (right flanks); tumours were allowed to grow for up to 17 days, and then were analysed on the Tpx3Cam PLIM imager on days 3, 7, 10 and 17 in vivo and immediately after animal's death. After this NanO2-IR distribution was analysed in fixed tumour tissues on the confocal PLIM microscope. Animals in control group (tumour size and phosphorescence background controls) were injected with non-stained CT26 cells. N = 6 in all animal groups. (**B**) Comparison of the growth rate of the control and stained tumours. (**C**) Intensity and PLIM images of NanO2-IR in live and euthanised animals on different days of tumour growth. (**D**) The O_2 concentration values of the probe in tumour regions of live and euthanised animals, taken with 6 min intervals on the different days of tumour growth (N = 3 in each group).

the rectal and IR thermometers, animal and tumour temperature during the imaging sessions stayed relatively con616161stant at around 30–33 °C (Figure S5, Supplementary Information). This allowed us to apply to all post-mortem images the O_2 calibration generated in vitro at 30 °C.

In the Main Trial, the end-point O_2 imaging analysis of animals was performed on days 3, 7, 10 and 17 of tumour growth (Fig. 2A). Grafted tumours stained with NanO2-IR were seen to grow approximately two times slower than those produced with unstained CT26 cells (Fig. 2B). This is in line with the above toxic effects of the probe on cells. By day 17, tumour size reached ~ 0.12 cm³, as compared to ~ 0.23 cm³ for control group. Figure 2C shows that at all stages of growth, tumour regions were clearly detectable on the intensity images, and this allowed accurate calculation of phosphorescence lifetime values. On the different days of tumour growth, mean lifetime values for standard 30 min imaging sessions performed on the different Days ranged between 44 and 52 µs, which correspond to tissue O_2 concentrations 25–0 µM, respectively (Fig. 2D). Similar $[O_2]$ profiles for individual animals (Mouse 1 from each group) are shown in Supplementary Figure S6.

The profile of mean $[O_2]$ over the whole period of tumour development and PLIM measurements under the Main Trial (Days 3, 7, 10 and 17; N = 3 animals for each time point, 6 measurements per animal) is shown in Fig. 3. Moreover, since the tumour growth and imaging conditions in the Preliminary Trial were identical to the Main Trial, the results of Preliminary Trial (i.e., mean $[O_2]$ on Days 4, 7 and 10; N = 3 animals for each time point, 6 measurements per animal) were also plotted on Fig. 3 and analysed as the second set of independent experiments. The two profiles show similar $[O_2]$ values, with a minor downward trend from Day 3 (or Day 4) to Day 10, and a prominent increase in tumour $[O_2]$ at the end of the Main Trial on Day 17. We attribute the latter effect to: (1) reduced O_2 consumption by tumours having large necrotic areas, which develop and expand in subcutaneous tumours on Day 14 and thereafter[60]; and (2) more heterogenous $[O_2]$ distribution, as 'a branched and chaotic vascular system' in the tumour becomes dominant on Day 17 after the injection of CT26 cells[61]. Indeed, the large variability of $[O_2]$ values measured on Day 17 (Fig. 3) supports this hypothesis.

However, statistical analysis of the PLIM data (Fig. 2D) did not reveal significant differences between tumours grown for different periods of time, likely because of the variability between animals and intratumoural processes. Lifetime values for the live animals ranged from ~ 44 µs (days 3 and 17) to ~ 46 µs (days 10 and 14), and the repeated measures ANOVA test did not show significant difference in lifetime values between PLIM images of live and post-mortem tumour tissue taken during each individual day of tumour growth. At the same time, ANOVA test showed a trend towards increased LT values in the euthanised vs live animals (see statistical details in Fig. 2C). The trend was particularly strong for day 17, with $p = 0.131$ for live vs dead mice.

It is generally accepted that soon after death, when blood circulation stops, tissue O_2 gets rapidly depleted. The observed little difference in NanO2-IR lifetime values between the live and euthanised animals on Days 7 and 10 of tumour progression, suggested that tissue oxygenation was rather low at these stages. And on Days 3 and 4 of the Main and Preliminary Trials, when tumours were not palpable, O_2 showed a positive trend compared to Days 7 and 10, but were still lower than on Day 17 (Fig. 2B). Day 3 of the Main Trial showed the highest variability of tissue $[O_2]$ values, the reasons of which are not clear. Similar effects were reported for the other cell models[62,63]. So, active proliferation of the injected CT26 cells during the initial engraftment phase can be accompanied by increased fraction of 'hypoxic cells inside the growing tumour', detectable by the imager.

Statistical analysis

The repeated measures ANOVA test was performed on the lifetime values recorded on the different days (shown in Fig. 2D), which shows:

(a) On day 3, for different imaging time $F(1.05, 2.1) = 1.89$, $p = 0.301$, with a mean of 43.7 µs for 0 min, 48.9 µs for 6 min, 50.59 µs for 12 min, 50.7 µs for 18 min, 51.38 µs for 24 min. $F = 5.2$, $p = 0.3857$ for 0 min vs 6 min; $F = 6.889$, $p = 0.2672$ for 0 min vs 12 min; $F = 6.999$, $p = 0.3215$ for 0 min vs 18 min; $F = 7.684$, $p = 0.2839$ for 0 min vs 24 min.
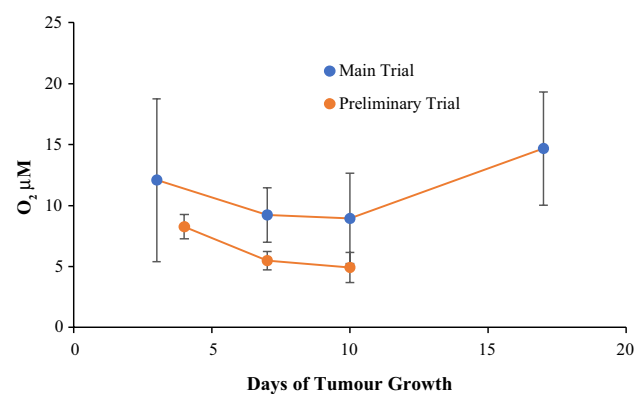

Figure 3. Dynamics of tumour oxygenation. Five PLIM images were taken at 6–30 min after animals were euthanised. Data of the Main and Preliminary Trials are presented. For each time point, N = 3 in both Trials.

(b) On day 7, for different imaging time, $F(1.45, 2.89) = 2.44$, $p = 0.232$, with a mean of 45.8 μs for 0 min, 50.1 μs for 6 min, 48.3 μs for 12 min, 48.1 μs for 18 min, 48.6 μs for 24 min. $F = 4.274$, $p = 0.2143$ for 0 min vs 6 min; $F = 2.515$, $p = 0.1808$ for 0 min vs 12 min; $F = 2.298$, $p = 0.165$ for 0 min vs 18 min; $F = 2.783$, $p = 0.2031$ for 0 min vs 24 min.

(c) On day 10, for different imaging time $F(4, 8) = 2.24$, $p = 0.154$, with a mean of 46.5 μs for 0 min, 47.4 μs for 6 min, 50.3 μs for 12 min, 49.4 μs for 18 min, 47.2 μs for 24 min. $F = 0.951$, $p = 0.2469$ for 0 min vs 6 min; $F = 3.8277$, $p = 0.144$ for 0 min vs 12 min; $F = 2.928$, $p = 0.2507$ for 0 min vs 18 min; $F = 0.7453$, $p = 0.5331$ for 0 min vs 24 min.

(d) On day 17, for different imaging time, $F(1.8, 3.59) = 3.79$, $p = 0.131$, with a mean of 43.8 μs for 0 min, 46.7 μs for 6 min, 45.3 μs for 12 min, 45.2 μs for 18 min, 46.0 μs for 24 min. $F = 2.85$, $p = 0.0746$ for 0 min vs 6 min; $F = 1.5387$, $p = 0.0214$ for 0 min vs 12 min; $F = 1.4177$, $p = 0.1182$ for 0 min vs 18 min; $F = 2.2347$, $p = 0.1981$ for 0 min vs 24 min.

Analysis of NanO2-IR distribution in tumour tissue

We also studied localisation of NanO2-IR in tumour tissue. For this, after the in vivo and post-mortem O_2 imaging sessions with animals, tumours were excised, fixed, sliced on a vibratome and then examined on a confocal PLIM microscope for the presence and distribution of the probe. In most cases, tissue areas containing NanO2-IR probe were detectable by visual examination, as darker spots (Fig. 4A). Further analysis confirmed the presence of NanO2-IR in these 'isles', surrounded most by non-stained tissue or tissue with low levels of the probe distributed diffusely. Such patchy distribution of the probe suggested that stained CT26 cells died soon after the injection and their debris formed these 'isles' of NanO2-IR probe, which were 0.1–3 mm in size (mostly 0.2–1 mm). The 'isles' were surrounded by actively growing non-stained cells, which produced tumours similar in size to the control (non-stained) tumours.

Using 3D image reconstructions, we also analysed LT signals across the stained 'isles' and found that they were independent on the probe concentration and aggregation (Fig. 4B,C). NanO2-IR 'isles' also remained unaffected during tumour growth: their size and average intensity signals were similar in tumour samples collected on days 10 and 17 (Fig. 4D, Fig. S3). The median lifetime values in the tissues collected at different stages of tumour growth also did not change and stayed at 22–24 μs. Upon chemical deoxygenation, the lifetimes increased to > 40 μs. This confirms the specificity of the observed phosphorescent signals from the probe, which were not affected by sample preparation, including the fixation with paraformaldehyde (Fig. 4E).
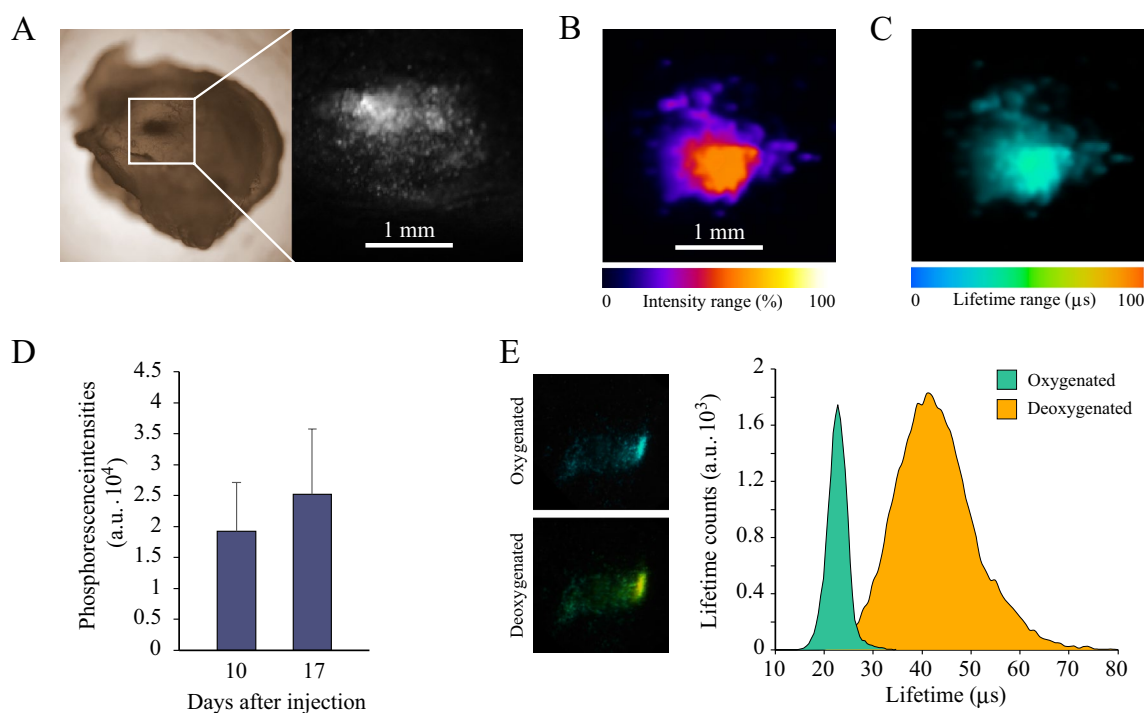
Figure 4. Analysis of NanO2-IR localisation in tumour tissue. (**A**) Representative image of tumour tissue with a NanO2-IR 'isle' positioned in the middle (left). The corresponding phosphorescence intensity image obtained by confocal PLIM microscopy (right, 5 × magnification). (**B, C**) Typical span of the phosphorescence intensity signals across the NanO2-IR 'isle' (B) and the corresponding lifetime values (C). (**D**) Analysis of the intensity signal of NanO2-IR residing in tumour tissue at different stages of tumour development (N = 6). (**E**) Response of NanO2-IR 'isle' to chemical deoxygenation of the tissue by sulphite. Right panel shows the typical shift of the distribution of lifetime values in response to decreased O_2 levels. Images represent stacks of six (**A–C**) or three (**E**) focal planes taken in 5 μm step.

Conclusions

The Tpx3Cam PLIIM imager and NanO2-IR probe showed promising performance in fast quantitative imaging of tissue hypoxia in animal models with grafted tumours. The conditions of NanO2-IR use in animals were optimised to minimise adverse effects of the probe on grafted tumours and enable long-term retention of the probe in grafts. The imager produced detailed lifetime maps that reflected hypoxic conditions in tumour regions, both in live and euthanised animals. The lifetime values measured in live animals ranged within 44–46 μs from day 3 to day 17 of tumour growth and showed no correlation with tumour progression. These results were in line with previous studies demonstrating profound hypoxia in the tumour tissue. The distribution of the NanO2-IR probe in the tumours and its LT signal in oxygenated and deoxygenated conditions were also examined by confocal PLIM microscopy of tissue samples which were excised on days 3–17. Compared to the other O_2 sensitive phosphorescent probes intended for intravital use, NanO2-IR was seen to be the most long-lasting probe, which produces stable and easily detectable intensity and lifetime signals for at least 17 days, little affected by tissue environment and tumour growth. Overall, the study demonstrated a fast, high-resolution, quantitative, minimally invasive method of PLIM imaging in physiological in-vivo studies.

Data availability

Data available on request from the corresponding author.

References

1. Schwartz, G. Ueber Desensibilisierung gegen rontgen und radiumstrahlen. *Munchener Medizinische Wochenschrift* **24**, 1–2 (1909).
2. Gray, L. H., Conger, A. D., Ebert, M., Hornsey, S. & Scott, O. C. The concentration of oxygen dissolved in tissues at the time of irradiation as a factor in radiotherapy. *Br. J. Radiol.* **26**, 638–648 (1953).
3. Thomlinson, R. H. & Gray, L. H. The histological structure of some human lung cancers and the possible implications for radiotherapy. *Br. J. Cancer* **9**, 539–549 (1955).
4. McKeown, S. R. Defining normoxia, physoxia and hypoxia in tumours—Implications for treatment response. *Br. J. Radiol.* **87**, 1–12 (2014).
5. Arbeit, J. M. *et al.* Hypoxia: Importance in tumor biology, noninvasive measurement by imaging, and value of its measurement in the management of cancer therapy. *Int. J. Radiat. Biol.* **82**, 699–757 (2006).
6. Vaupel, P., Höckel, M. & Mayer, A. Detection and characterization of tumor hypoxia using pO2 histography. *Antioxid. Redox Signal.* **9**, 1221–1235 (2007).
7. Emami Nejad, A. *et al.* The role of hypoxia in the tumor microenvironment and development of cancer stem cell: A novel approach to developing treatment. *Cancer Cell Int.* **21**, 1–26 (2021).
8. Singleton, D. C., Macann, A. & Wilson, W. R. Therapeutic targeting of the hypoxic tumour microenvironment. *Nat. Rev. Clin. Oncol.* **18**, 751–772 (2021).
9. Masoud, G. N. & Li, W. HIF-1α pathway: role, regulation and intervention for cancer therapy. *Acta Pharmaceutica Sin. B* **5**, 378–389 (2015).
10. Liu, Z. G. & Jiao, D. Necroptosis, tumor necrosis and tumorigenesis. *Cell Stress* **4**, 1–8 (2020).
11. Galluzzi, L. *et al.* Molecular mechanisms of cell death: Recommendations of the Nomenclature Committee on Cell Death 2018. *Cell Death Differ.* **25**, 486–541 (2018).
12. Richards, C. H., Mohammed, Z., Qayyum, T., Horgan, P. G. & McMillan, D. C. The prognostic value of histological tumor necrosis in solid organ malignant disease: A systematic review. *Future Oncol.* **7**, 1223–1235 (2011).
13. Carreau, A., Hafny-Rahbi, B. E., Matejuk, A., Grillon, C. & Kieda, C. Why is the partial oxygen pressure of human tissues a crucial parameter? Small molecules and hypoxia. *J. Cell. Med. Mol.* **15**, 1239–1253 (2011).
14. Sun, X., Niu, G., Chan, N., Shen, B. & Chen, X. Tumor hypoxia imaging. *Mol. Imag. Biol.* **13**, 399–410 (2011).
15. Serganova, I., Humm, J., Ling, C. & Blasberg, R. Tumor hypoxia imaging. *Clin. Cancer Res.* **12**, 5260–5264 (2006).
16. Clark, L. C. C. Jr. Monitor and control of blood and tissue oxygen tensions. *Trans. Am. Soc. Artif. Intern. Organs* **2**, 41–48 (1956).
17. Bartlett, K., Saka, M. & Jones, M. Polarographic electrode measures of cerebral tissue oxygenation: Implications for functional brain imaging. *Sensors (Basel, Switzerland)* **8**, 7649–7670 (2008).
18. Stone, H. B., Brown, J. M., Phillips, T. L. & Sutherland, R. M. Oxygen in human tumors: Correlations between methods of measurement and response to therapy. Summary of a workshop held November 19–20, 1992, at the National Cancer Institute, Bethesda, Maryland. *Radiation research* **136**, 422–434 (1993).
19. Fleming, I. N. *et al.* Imaging tumour hypoxia with positron emission tomography. *Br. J. Cancer* **112**, 238–250 (2015).
20. Koch, C. J. & Evans, S. M. Non-invasive pet and spect imaging of tissue hypoxia using isotopically labeled 2-nitroimidazoles. *Adv. Exp. Med. Biol.* **510**, 285–292 (2003).
21. Gambhir, S. S. Molecular imaging of cancer with positron emission tomography. *Nat. Rev. Cancer* **2**, 683–693 (2002).
22. Holland, J. P., Lewis, J. S. & Dehdashti, F. Assessing tumor hypoxia by positron emission tomography with Cu-ATSM. *Q. J. Nucl. Med. Mol. Imag.* **53**, 193–200 (2009).
23. Boushel, R. *et al.* Monitoring tissue oxygen availability with near infrared spectroscopy (NIRS) in health and disease. *Scand. J. Med. Sci. Sports* **11**, 213–222 (2001).
24. Boushel, R. & Piantadosi, C. A. Near-infrared spectroscopy for monitoring muscle oxygenation. *Acta Physiol. Scand.* **168**, 615–622 (2000).
25. Intes, X. & Chance, B. Non-PET functional imaging techniques: Optical. *Radiol. Clin. N. Am.* **43**, 221–34 (2005).
26. Nioka, S. & Chance, B. NIR spectroscopic detection of breast cancer. *Technol. Cancer Res. Treat.* **4**, 497–512 (2005).
27. Li, M., Tang, Y. & Yao, J. Photoacoustic tomography of blood oxygenation: A mini review. *Photoacoustics* **10**, 65–73 (2018).
28. Cao, F., Qiu, Z., Li, H. & Lai, P. Photoacoustic imaging in oxygen detection. *Appl. Sci.* **7**, 1262 (2017).
29. Danielli, A., Favazza, C. P., Maslov, K. & Wang, L. V. Single-wavelength functional photoacoustic microscopy in biological tissue. *Opt. Lett.* **36**, 769–771 (2011).
30. Li, M.-L. *et al.* Simultaneous molecular and hypoxia imaging of brain tumors in vivo using spectroscopic photoacoustic tomography. *Proc. IEEE* **96**, 481–489 (2008).
31. Busse, L. J., Pratt, R. G. & Thomas, S. R. Deconvolution of chemical shift spectra in two- or three-dimensional [19F] MR imaging. *J. Comput. Assist. Tomogr.* **12**, 824–835 (1988).
32. Mason, R. P. *et al.* Non-invasive determination of tumor oxygen tension and local variation with growth. *Int. J. Radiat. Oncol. Biol. Phys.* **29**, 95–103 (1994).

33. Tirotta, I. *et al.* 19F magnetic resonance imaging (MRI): From design of materials to clinical applications. *Chem. Rev.* **115**, 1106–1129 (2015).
34. Li, L.-P., Halter, S. & Prasad, P. V. Blood oxygen level-dependent MR imaging of the kidneys. *Magn. Reson. Imag. Clin. N. Am.* **16**, 613–25 (2008).
35. Stacy, M. R. *et al.* Application of BOLD magnetic resonance imaging for evaluating regional volumetric foot tissue oxygenation: A feasibility study in healthy volunteers. *Eur. J. Vasc. Endovasc. Surg.* **51**, 743–749 (2016).
36. Baudelet, C. & Gallez, B. How does blood oxygen level-dependent (BOLD) contrast correlate with oxygen partial pressure (pO2) inside tumors?. *Magn. Reson. Med.* **48**, 980–986 (2002).
37. Gordon, Y. *et al.* Dynamic contrast-enhanced magnetic resonance imaging: fundamentals and application to the evaluation of the peripheral perfusion. *Cardiovasc. Diagn. Ther.* **4**, 147–164 (2014).
38. Nielsen, T., Wittenborn, T. & Horsman, M. R. Dynamic contrast-enhanced magnetic resonance imaging (DCE-MRI) in preclinical studies of antivascular treatments. *Pharmaceutics* **4**, 563–589 (2012).
39. Taylor, J. S. *et al.* MR imaging of tumor microcirculation: Promise for the new millennium. *J. Magn. Reson. Imag.* **10**, 903–907 (1999).
40. Swartz, H. M. Using EPR to measure a critical but often unmeasured component of oxidative damage: Oxygen. *Antioxid. Redox Signal.* **6**, 677–686 (2004).
41. Mallard, J. R. & Kent, M. Electron spin resonance in biological tissues. *Phys. Med. Biol.* **14**, 373–396 (1969).
42. Klare, J. P. Biomedical applications of electron paramagnetic resonance (EPR) spectroscopy. *Biomed. Spectrosc. Imag.* **1**, 101–124 (2012).
43. Rumsey, W. L., Vanderkooi, J. M. & Wilson, D. F. Imaging of phosphorescence: A novel method for measuring oxygen distribution in perfused tissue. *Science* **241**, 1649–1651 (1988).
44. Wilson, D. F., Rumsey, W. L. & Vanderkooi, J. M. Oxygen distribution in isolated perfused liver observed by phosphorescence imaging. *Adv. Exp. Med. Biol.* **248**, 109–115 (1989).
45. Vinogradov, S. A. *et al.* Oxygen distributions in tissue measured by phosphorescence quenching. *Adv. Exp. Med. Biol.* **510**, 181–185 (2003).
46. Dunphy, I., Vinogradov, S. A. & Wilson, D. F. Oxyphor R2 and G2: Phosphors for measuring oxygen by oxygen-dependent quenching of phosphorescence. *Anal. Biochem.* **310**, 191–198 (2002).
47. Wilson, D. F., Vinogradov, S. A., Schears, G. J., Esipova, T. V. & Pastuszko, A. Monitoring cardiopulmonary function and progression toward shock: Oxygen micro-sensor for peripheral tissue. *Adv. Exp. Med. Biol.* **737**, 221–227 (2012).
48. Sakadžić, S. *et al.* Two-photon high-resolution measurement of partial pressure of oxygen in cerebral vasculature and tissue. *Nature Methods* **7**, 755–759 (2010).
49. Esipova, T. V. *et al.* Oxyphor 2P: A high-performance probe for deep-tissue longitudinal oxygen imaging. *Cell Metab.* **29**, 736-744.e7 (2019).
50. Tsytsarev, V. *et al.* In vivo imaging of brain metabolism activity using a phosphorescent oxygen-sensitive probe. *J. Neurosci. Methods* **216**, 146–151 (2013).
51. Dmitriev, R. I., Zhdanov, A. V., Jasionek, G. & Papkovsky, D. B. Assessment of cellular oxygen gradients with a panel of phosphorescent oxygen-sensitive probes. *Anal. Chem.* **84**, 2930–2938 (2012).
52. Sen, R. *et al.* New luminescence lifetime macro-imager based on a Tpx3Cam optical camera. *Biomed. Opt. Express* **11**, 77–88 (2020).
53. Trettnak, W. *et al.* Optical oxygen sensor instrumentation based on the detection of luminescence lifetime. *Adv. Space Res.* **22**, 1465–1474 (1998).
54. Sen, R. *et al.* A new macro-imager based on Tpx3Cam optical camera for PLIM applications. *Proc. SPIE 11359, Biomedical Spectroscopy, Microscopy, and Imaging* **113591N**, 60 (2020).
55. Sen, R. *et al.* Characterization of planar phosphorescence based oxygen sensors on a TCSPC-PLIM macro-imager. *Sens. Actuators, B: Chem.* **321**, 128459 (2020).
56. Sen, R. *et al.* Mapping O2 concentration in ex-vivo tissue samples on a fast PLIM macro-imager. *Sci. Rep.* **10**, 1–11 (2020).
57. Fercher, A., Borisov, S. M., Zhdanov, A. V, Klimant, I. & Papkovsky, D. B. Intracellular O_2 Sensing Probe Based on Cell-Penetrating Phosphorescent Nanoparticles. *ACS Nano* **5**, 5499–5508 (2011).
58. Dmitriev, R. I., Zhdanov, A. V., Nolan, Y. M. & Papkovsky, D. B. Imaging of neurosphere oxygenation with phosphorescent probes. *Biomaterials* **34**, 9307–9317 (2013).
59. Hedenstierna, G. & Edmark, L. Effects of anesthesia on the respiratory system. *Best Pract. Res. Clin. Anaesthesiol.* **29**, 273–284 (2015).
60. Lukina, M. M. *et al.* Effects of irinotecan on tumor vasculature and oxygenation: An in vivo study on colorectal cancer model. *IEEE J. Sel. Top. Quantum Electr.* **27**, 1–8 (2020).
61. Haedicke, K. *et al.* High-resolution optoacoustic imaging of tissue responses to vascular-targeted therapies. *Nat. Biomed. Eng.* **4**, 286–297 (2020).
62. Hoffmann, B. *et al.* The initial engraftment of tumor cells is critical for the future growth pattern: A mathematical study based on simulations and animal experiments. *BMC Cancer* **20**, 524 (2020).
63. Bertin, H., Udo, S. & Gero, W. Absence of convection in solid tumors caused by raised interstitial fluid pressure severely limits success of chemotherapy—A numerical study in cancers. *Math. Biosci. Eng.* **17**(5), 6128–6148 (2020).

Acknowledgements

Author contributions

A.V.Z. planned the study and prepared the cells. C.D. was responsible for the experiments in animals. R.S. performed in vivo imaging on animals. L.L. performed the confocal microscopy, thermometry and probe calibration. Original draft preparation was conducted by R.S. and A.V.Z. Writing, reviewing, and editing of the draft manuscript was completed by A.V.Z., R.S. and D.B.P. Visualization and figure creation was completed by A.V.Z. and R.S. All authors commented on previous versions of the manuscript. All authors read and approved the final manuscript.

Funding

Competing interests

The authors declare no competing interests.

Additional information

Supplementary Information The online version contains supplementary material available at https://doi.org/10.1038/s41598-023-46224-7.

Correspondence and requests for materials should be addressed to D.B.P.

Reprints and permissions information is available at www.nature.com/reprints.

Publisher's note Springer Nature remains neutral with regard to jurisdictional claims in published maps and institutional affiliations.